Development/Plasticity/Repair

Postnatal Development of Intrinsic and Synaptic Properties Transforms Signaling in the Layer 5 Excitatory Neural Network of the Visual Cortex

Sarah J. Etherington[1,2] **and Stephen R. Williams**[1,3]

[1]Medical Research Council Laboratory of Molecular Biology, Cambridge CB2 OQH, United Kingdom, [2]Murdoch University, Murdoch 6150, Australia, and [3]Queensland Brain Institute, University of Queensland, St. Lucia 4072, Australia

Information flow in neocortical circuits is regulated by two key parameters: intrinsic neuronal properties and the short-term activity-dependent plasticity of synaptic transmission. Using multineuronal whole-cell voltage recordings, we characterized the postnatal maturation of the electrophysiological properties and short-term plasticity of excitatory synaptic transmission between pairs of layer 5 (L5) pyramidal neurons ($n = 158$) in acute slices of rat visual cortex over the first postnatal month. We found that the intrinsic and synaptic properties of L5 pyramidal neurons develop in parallel. Before postnatal day 15 (P15), intrinsic electrophysiological properties were tuned to low-frequency operation, characterized by high apparent input resistance, a long membrane time constant, and prolonged somatic action potentials. Unitary excitatory synaptic potentials were of large amplitude (P11–P15; median, 514 μV), but showed pronounced use-dependent depression during prolonged regular and physiologically relevant presynaptic action potential firing patterns. In contrast, in mature animals we observed a developmental decline of the peak amplitude of unitary EPSPs (P25–P29; median, 175 μV) paralleled by a decrease in apparent input resistance, membrane time constant, and somatic action potential duration. Notably, synaptic signaling of complex action potential firing patterns was also transformed, with P25–P29 connections faithfully signaling action potential trains at frequencies up to 40 Hz (1st to 50th action potential ratio, 0.91 $\pm$ 0.12). Postnatal refinement of intrinsic properties and short-term plasticity therefore transforms the capacity of the L5 excitatory neural network of the visual cortex to generate and process patterns of action potential firing and contribute to network activity.

Introduction

The functional unit underlying the brain's higher cognitive functions is the neocortical microcircuit (Douglas and Martin, 2004). During the first postnatal month in rodents, the neocortical microcircuit is anatomically and functionally reorganized (McCormick and Prince, 1987; Kasper et al., 1994a; Micheva and Beaulieu, 1996; DeFelipe, 1997; Franceschetti et al., 1998; for review, see Cohen-Cory, 2002; van Zundert et al., 2004; Zhang, 2004). Consequently, network activity generated within the neocortical microcircuit is dramatically refined over this developmental period (Yuste et al., 1992; Chiu and Weliky, 2002; Khazipov et al., 2004; Golshani et al., 2009; Rochefort et al., 2009). As synchronized neocortical network activity is believed to be initiated and propagated by networks of layer 5 (L5) pyramidal neurons (Silva et al., 1991; Sanchez-Vives and McCormick, 2000; Sakata and Harris, 2009), investigation of the postnatal development of the intrinsic properties and intracortical synaptic connectivity of these neurons is critical to an understanding how coherent neocortical network activity is generated and refined during early postnatal life.

In sensory cortices, the first postnatal month also encompasses a number of functional milestones. In rodent visual cortex, these include the emergence of ocular dominance, orientation, and movement selectivity; refinement in cortical neuron receptive fields; and increased visual acuity (Fagiolini et al., 1994). Any change in the spread of activity through neocortical circuits due to maturational changes in the intrinsic properties of neurons and/or synaptic transmission would potentially shape cortical developmental milestones, because many developmental processes are at least partially dependent on the level and/or pattern of activity in neocortical circuits (Katz and Shatz, 1996; Huberman et al., 2008). The impact of this dynamic interaction between neocortical activity, developmental milestones, and intrinsic and synaptic properties is likely to be most relevant in sensory cortices, where activity in afferent pathways changes rapidly in association with the development of peripheral sensory structures (Wong, 1999; Akerman et al., 2002; Fiser et al., 2004; Rochefort et al., 2009). The enduring impact of these early developmental interactions on cognitive functioning in adulthood are being increasingly recognized (Rice and Barone, 2000).

We have therefore characterized age-dependent changes in the intrinsic electrophysiological and synaptic properties of L5

Received Jan. 26, 2011; revised April 29, 2011; accepted May 18, 2011.

Author contributions: S.J.E. and S.R.W. designed research; S.J.E. performed research; S.J.E. and S.R.W. analyzed data; S.J.E. and S.R.W. wrote the paper.

This work was supported by the Medical Research Council (United Kingdom) and the Australian Research Council.

Correspondence should be addressed to either of the following: Dr. Sarah Etherington, School of Veterinary and Biomedical Sciences, Murdoch University, South Street, Murdoch, Western Australia, 6150, Australia, E-mail: s.etherington@murdoch.edu.au; or Stephen Williams, The Queensland Brain Institute, University of Queensland, QBI Building, #79, St Lucia, Queensland, 4072, Australia, E-mail: srw@uq.edu.au.

DOI:10.1523/JNEUROSCI.0458-11.2011

 0270-6474/11/319526-12$15.00/0

pyramidal networks in the rodent visual cortex. Using multineuronal current-clamp recordings, we show that the ability of L5 synapses to transmit complex action potential (AP) firing patterns is transformed over the first postnatal month, a change that is paralleled by a developmental refinement of intrinsic neuronal properties. Such postnatal maturation is likely to have widespread implications for information transfer within the neocortical column. These changes may also have a significant downstream impact on the spread of activity through subcortical circuits, as large L5 pyramidal neurons provide the main output of the microcircuit to subcortical targets (Solomon and Nerbonne, 1993a,b; Wang and McCormick, 1993; Albert and Nerbonne, 1995).

Materials and Methods

All experiments were conducted in accordance with institutional and UK Home Office guidelines.

Slice preparation and maintenance. Whole-cell, current-clamp recordings were made from slices of visual cortex prepared from male Long Evans rats [postnatal day 7 (P7)–P29]. All animals were housed with artificial 12 h light/dark cycles, and animals younger than P15 were photographed before euthanasia to document the level of eye opening. Littermates were housed together; dams were removed from cages at weaning (P21). Animals were anesthetized by inhalation of isoflurane and then decapitated. Brains were rapidly removed and submerged in an oxygenated (95% oxygen, 5% carbon dioxide) chilled slicing solution containing the following (in mM): 125 NaCl, 25 $NaHCO_3$, 3 KCl, 1.25 NaH_2PO_4, 1 $CaCl_2$, 6 $MgCl_2$, 3 sodium pyruvate, and 25 glucose, pH 7.4. The cerebellum and the brain frontal to the central sulcus were removed, and 300 μm slices of occipital neocortex were cut with a vibratome at an angle of 15° relative to the coronal plane. Slices were maintained at 35°C for 30 min in a holding chamber containing oxygenated slicing solution and then allowed to cool to room temperature (21–24°C). Recordings were made between 1 and 8 h after slice preparation.

Electrophysiological recording. Individual brain slices were transferred to the bath of an upright Olympus BX51WI microscope and perfused at 2 $ml \cdot min^{-1}$ with an oxygenated recording solution containing the following (in mM): 125 NaCl, 25 $NaHCO_3$, 3 KCl, 1.25 NaH_2PO_4, 2 $CaCl_2$, 1 $MgCl_2$, 3 sodium pyruvate, and 25 glucose, pH 7.4 (35–37°C). Whole-cell somatic voltage recordings were made with borosilicate glass recording pipettes with resistances between 3 and 8 MΩ when filled with solution composed of the following (in mM): 135 K-gluconate, 7 NaCl, 10 HEPES, 2 Na2ATP, 0.3 NaGTP, 2 $MgCl_2$, and 0.01 Alexa Fluor 488, adjusted to pH 7.3 with KOH. Dual and triple whole-cell current-clamp recordings were made with identical bridge-balance amplifiers (Dagan BVC 700A). Current and voltage signals were low-pass filtered (DC to 10 kHz) and acquired at 30–50 kHz with an ITC-18 (Instrutech Corporation) interface controlled by an Apple computer. Signal acquisition and analysis were performed with Axograph software (Molecular Devices). Series resistance was regularly monitored and adjusted throughout each experiment. Recordings were abandoned if the postsynaptic series resistance increased above 25 MΩ or changed by >20%.

Recordings were targeted to large, thick-tufted L5 pyramidal neurons using infrared differential interference contrast microscopy. Thick-tufted L5 neurons can be distinguished from slender L5 neurons by the end of the first postnatal week based on their thick apical dendrite and the presence of a dendritic tuft in L1 (Jones and Wise, 1977; Kasper et al., 1994b).

To locate synaptically connected neurons, simultaneous whole-cell recordings were made from two or three closely spaced L5 pyramidal neurons (soma to soma distance, <40 μm). Synaptic connectivity was assessed between each pair of neurons sequentially by repeatedly eliciting pairs of action potentials in a neuron (2 ms test pulses; 1–5 nA; 30 ms paired-pulse interval; 20 sweeps delivered at 0.33 Hz). If a synaptic connection was not identified after each neuron had been investigated, one electrode was withdrawn, and a whole-cell recording was established with a new pyramidal neuron.

Once a synaptically connected pair of neurons was identified, a variety of simple and complex stimulus trains were delivered to the presynaptic neuron until the series resistance or the cell quality deteriorated. Resting membrane potential was recorded within 1 min of attaining a whole-cell recording and corrected for the offset potential recorded when then electrode was detached from the neuron at the end of each experiment. Square-wave current pulses were used to elicit small depolarizing and hyperpolarizing voltage responses (200 sweeps, intersweep interval, 0.3 s; 200 ms stimulus duration; current amplitudes selected to produce voltage deflection <5 mV; average amplitude, 4.2 ± 0.2 mV; $n = 55$ cells). Membrane time constant was taken as the second (longer) time constant of a double exponential fit to the charging of voltage responses. Current–voltage relationships were determined using long, square-wave current steps of varying amplitude and polarity (800 ms; intersweep interval, 30 s). At least two sweeps were averaged for each stimulus level to obtain the final voltage response. The peak voltage response was calculated from the average amplitude within a 0.5 ms window around the peak voltage deflection. The steady-state voltage response was the average voltage deflection occurring during the last 20 ms of the stimulus. Apparent input resistance was estimated from the slope of a regression line fitted to the linear portion of the peak current–voltage relationship.

Action potential properties were derived from recordings of single action potentials evoked by 100 ms square-wave pulses at rheobase current (the minimum somatic current required to evoke an action potential, 20 sweeps delivered at 0.5 Hz). Reported values are the average parameters of at least three action potentials from each neuron. Action potential threshold was defined as the membrane potential at a time point just before the derivative of the action potential increased rapidly above baseline during the action potential upstroke.

Unitary EPSP (uEPSP) amplitude was estimated by measuring the amplitude over a 0.2 or 0.5 ms time window centered around the uEPSP peak relative to a baseline window 0.5 ms before stimulus onset. Unitary EPSP failure rates were calculated by counting the number of sweeps in which presynaptic action potential firing did not produce a time-locked postsynaptic response (minimum of 100 sweeps per connection tested). Paired-pulse properties were estimated by interleaving the generation of a single or pair of presynaptic action potentials (2 ms pulses of 1–5 nA; 25 ms paired-pulse interval; 200 sweeps delivered at 0.2 Hz). The paired-pulse ratio (PPR) was calculated by averaging the responses to single and paired stimuli and then digitally subtracting the single uEPSP waveform from the double uEPSP waveform.

Histology. At the conclusion of each experiment, digital fluorescent images of live cells were captured using a Retiga EXI camera (QImaging) mounted to the BX51 microscope. Each slice was removed from the recording chamber, washed in PBS, and fixed overnight at 4°C in 4% paraformaldehyde (in PBS). Fixed slices were rinsed briefly in distilled, deionized water and mounted on microscope slides with Vectashield mounting medium (Vector Laboratories). Gray-scale projections of fixed, recorded neurons were constructed from 1 μm optical sections captured with a Bio-Rad Radiance 2000 confocal system.

Statistical analysis. Numerical values are expressed as mean ± SEM unless indicated otherwise. Statistical significance was determined with two-tailed Student's *t* tests or two-way ANOVAs with Bonferroni post-tests for parametric data. Kolmogorov–Smirnov or Mann–Whitney *U* tests were performed to determine statistical significance for nonparametric data.

Results

Dual or triple whole-cell somatic current-clamp recordings were made from large, thick-tufted L5 pyramidal neurons in acute slices of primary and secondary visual cortex from hooded rats aged P7–P29. Most recordings were targeted to two developmental periods, P11–P15 and P25–P29. Unitary EPSPs were recorded from 159 monosynaptically connected pairs of neurons. Twelve of these monosynaptically connected pairs of neurons were reciprocally connected, of which eight were observed in cortical slices from animals age P12 or younger.

Development of intrinsic membrane properties

Early postnatal development is associated with rapid and substantial changes in the intrinsic membrane properties of neocortical neurons (McCormick and Prince, 1987; Zhang, 2004; Frick et al., 2007a; Oswald and Reyes, 2008), which will profoundly influence local network activity. In our study, the apparent input resistance (R_{in}) of L5 pyramidal neurons decreased significantly between P11 and P29, with the most rapid change occurring during the second postnatal week (mean R_{in}: P11, 163 ± 18 MΩ, $n = 6$; P15, 75 ± 11 MΩ, $n = 6$; P25–P29, 62 ± 4 MΩ, $n = 6$; $p < 0.001$, Kruskal–Wallis test) (Fig. 1*A*,*B*). The estimated membrane time constant (τ_c) decreased from 29.3 ± 2.6 ms ($n = 9$) to 23.5 ± 3.0 ms ($n = 12$) between P11 and P15, and then continued to fall during the third postnatal week to reach a mature level of 12.9 ± 5.0 ms (derived from the plateau of a single exponential function fitted to the data in Fig. 1*C*) (decay constant, 6.19 d; $n = 55$ cells). A strong positive correlation was observed between τ_c and R_{in} when data were pooled across age groups ($r^2 = 0.731$; $p < 0.0001$; $n = 61$; data not shown), consistent with a developmental decrease in specific membrane resistivity accelerating the membrane time constant and contributing to the decline in R_{in}.

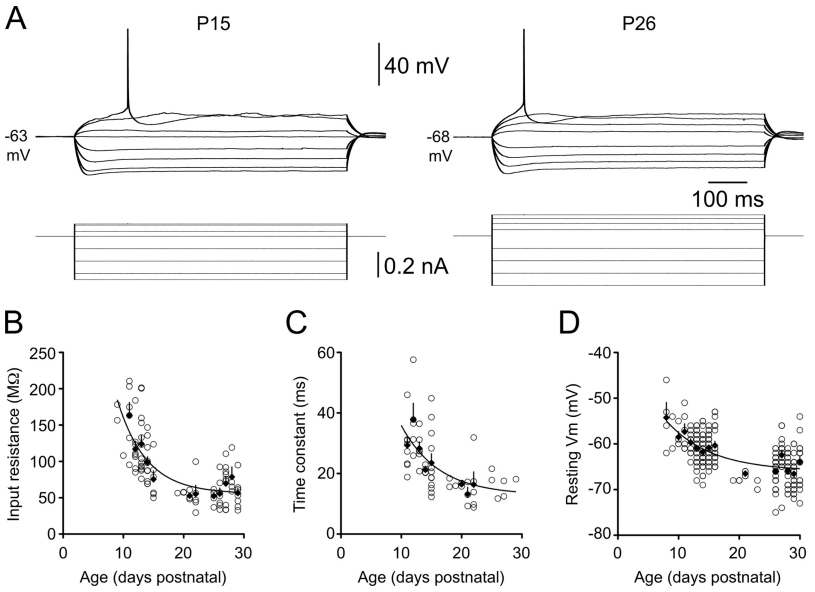

Figure 1. Postnatal development of the subthreshold membrane properties of layer 5 pyramidal neurons. ***A***, Voltage responses (top traces) generated by steps of injected current (bottom traces) recorded from representative P15 (left) and P26 (right) layer 5 pyramidal neurons. Note the developmental decrease in apparent input resistance and increase in rheobase current. Action potentials have been truncated. ***B–D***, Summary graphs show age-dependent decreases in apparent input resistance (***B***), membrane time constant (***C***), and resting membrane potential (***D***). Each data point represents an individual layer 5 pyramidal neuron. Filled diamonds are averages for each postnatal day. Error bars indicate SEM. Trend lines represent single exponential fits to the data.

A small but significant hyperpolarization of the resting membrane potential (V_m) emerged gradually over the same period (Fig. 1*D*). While resting V_m did not change significantly between P11 and P15 ($p = 0.661$), the average V_m at P25–P29 (−65.1 ± 0.38 mV; $n = 98$) was ~4 mV more negative than the average V_m at P11–P15 (−60.9 ± 0.33 mV; $n = 105$; $p < 0.0001$, two-tailed t test).

Development of action potential properties

Between P11 and P15, the period over which subthreshold membrane properties were transformed (Fig. 1*B*,*C*), AP waveforms in L5 pyramidal neurons matured rapidly (Table 1; Fig. 2*A*, representative traces). Over this 4 d period, AP amplitude increased by 8% (Fig. 2*B*), and the peak AP derivative increased by 33% (Fig. 2*C*), whereas AP rise time decreased by 15% (Fig. 2*D*), and AP half-width decreased by 50% (Fig. 2*E*; see Table 1 for numerical values). As an example of the speed of maturation of AP time course, a single exponential fit to half-width data revealed a mature value 0.679 ± 0.02 ms, which was reached with an age constant of only 3.21 d (P9–P29; $r^2 = 0.809$; $n = 67$) (Fig. 2*E*, curve).

Action potential after potentials became multiphasic during postnatal development, consistent with other studies of developing cortical neurons (McCormick and Prince, 1987; Franceschetti et al., 1998). A single prolonged (>50 ms) afterhyperpolarization potential was observed in L5 pyramidal neurons during the second postnatal week (Fig. 2*A*, left), whereas three distinct afterpotentials were apparent by the fourth postnatal week (a brief hyperpolarizing potential, a brief depolarizing potential, and the sustained hyperpolarization potential) (Fig. 2*A*, right). The amplitude of the slow afterhyperpolarization potential did not change significantly between the second and fourth postnatal weeks (Table 1). Overall, somatically recorded AP parameters were relatively stable after P15, suggesting that voltage-gated sodium and potassium conductances underlying APs approach mature levels by the end of the second postnatal week.

The threshold for AP firing (V_t) (Fig. 2*A*, gray lines) in L5 pyramidal neurons decreased rapidly from −39.5 ± 0.94 mV in P11 animals to −44.8 ± 0.98 mV in P15 animals ($p = 0.0037$; two-tailed t test), with no further change in V_t observed during the period studied (average V_t in animals aged P25–P29, −45.4 ± 0.77 mV). The rheobase current increased approximately threefold between P11 and P29 (Fig. 2*F*). Our results support the developmental reduction in R_{in} as the primary contributor to this decrease in neuronal excitability. The difference between V_m and V_t did not change significantly over this period (Table 1), while the inverse of R_{in} (conductance) was correlated with, and explained a substantial proportion of the variance in, rheobase across the developmental period ($r^2 = 0.458$; $p = 4.9 \times 10^{-11}$; $n = 73$ cells; data not shown).

Development of the properties of unitary synaptic potentials

The amplitude of monosynaptic L5–L5 unitary EPSPs evoked by a single presynaptic action potential decreased approximately threefold between postnatal weeks 1 and 4, from a median amplitude of 514 μV at P11–P15 to a median amplitude of only 175 μV at P25–P29 ($p < 0.0001$, two-tailed Mann–Whitney U) (Fig. 3*A*, traces, *B*, summary data, *D*, morphological development of neuronal pairs). While this rapid decline in uEPSP amplitude occurred contemporaneously with the developmental reduction in R_{in} (Fig. 1*B*), across the data set uEPSP amplitude was not correlated with postsynaptic R_{in} (r^2 of linear regression line, 0.107; slope not significantly different from zero; $p = 0.067$) (Fig. 3*C*). Notably, unlike intrinsic neuronal properties, developmental modification of uEPSP amplitude appeared to be biphasic. An abrupt increase in uEPSP amplitude was documented at ~P10–

Table 1. Postnatal maturation of action potential properties

	Age (days postnatal)		
Property	P11	P15	P25–P29
AP threshold (mV)	−39.5 ± 0.94 (5)	−44.8 ± 0.95 (9)*	−45.4 ± 0.77 (19)*
Relative AP threshold (mV above V_m)	24.0 ± 0.81 (5)	21.7 ± 1.4 (9)	24.1 ± 1.0 (19)
AP amplitude (mV above threshold)	75.7 ± 3.0 (5)	82.1 ± 1.8 (9)	84.8 ± 1.4 (19)*
AP rise time 10–90% (ms)	0.246 ± 0.014 (5)	0.214 ± 0.0083 (9)	0.194 ± 0.0065 (19)**
AP half-width (ms)	1.18 ± 0.082 (5)	0.786 ± 0.020 (9)	0.680 ± 0.020 (19)***,#
Peak AP derivative ($V_s - 1$)	314 ± 29 (5)	419 ± 27 (9)	475 ± 17 (21)**
Slow AHP amplitude (mV)	−13.0 ± 0.83 (5)	−8.74 ± 1.5 (9)**	−8.91 ± 0.46 (17)*

All results are shown as mean ± SEM (*n*). Significance was determined by nonparametric Kruskal–Wallis test followed by Dunn's multiple comparison post-tests. Overall differences were statistically significant ($p < 0.05$) for all variables except for relative AP threshold ($p = 0.374$). Action potential and afterhyperpolarizing potential (AHP) amplitudes are expressed relative to AP threshold (V_t).

*$p < 0.05$; **$p < 0.01$; ***$p < 0.001$ (significantly different from P11 level); #$p < 0.05$ (significantly different from P15 level).

P11, followed by a decline in uEPSP amplitude over the period P11–P29 (Fig. 3*B*).

The protracted decline in uEPSP amplitude from P11 to P29 could be largely attributed to an age-related decrease in release probability (p_r). The uEPSP failure rate (see Material and Methods) increased approximately fourfold from a median of 9% (range, 0–69%; $n = 52$) at P11–P15 to a median of 38% at P25–P29 (range, 0–76%; $n = 49$; $p < 0.0001$, two-tailed Mann–Whitney *U*) (Figs. 4*A*, 7*A*, traces). When failures were excluded from analysis of uEPSP amplitude, the median nonfailure uEPSP amplitude in P11–P15 animals was 11% higher than the average amplitude including failures, whereas exclusion of failures in P25–P29 animals resulted in a 39% increase in the median uEPSP amplitude (data not shown). Similarly, the coefficient of variation (CV) of uEPSP amplitude almost doubled over the same period, from 0.511 at P11–P15 (range 0.17–1.96) to 0.970 at P25–P29 (range, 0.27–3.06; $p < 0.0001$, two-tailed Mann–Whitney *U*) (Fig. 4*B*). When data were pooled across the two age groups, a relationship between uEPSP amplitude and CV was revealed (Fig. 4*C*). These data could be described by a single binomial model given by the equation $CV = \sqrt{[(1 - p_r)/(n_b p_r)}$, assuming that $CV = \Delta V/(n_b q_s)$ and the number of transmitter release sites, n_b, equals 5.5 (Markram et al., 1997). The sum of squared differences between the model and our CV measurements was minimized when the somatic quantal amplitude, q_s, was 0.23. The equation provided a good fit to data from all age groups (Fig. 4*C*, black dashed line) when uEPSP amplitude was <1 mV, arguing against a developmental change in quantal content. This finding and the observed developmental decrease in synaptic efficacy and reliability are consistent with a reduction in p_r between postnatal weeks 2 and 4 being the main contributor to the marked maturational decrease in uEPSP amplitude.

The kinetics of uEPSPs accelerated between P11–P15 and P25–P29. The rise time of uEPSPs decreased by ~35% over this period, from a median of 2.54 ms at P11–P15 (range, 0.9–7.9 ms) (Fig. 5*A*, traces in inset) to a median of 1.68 ms at P25–P29 (range, 0.7–5.56; $p = 0.0002$, two-tailed Mann–Whitney *U*), whereas the half-width fell from a median value of 27.0 ms (range, 12.0–80.6 ms) to 14.5 ms (range, 6.67–28.1 ms; $p < 0.0001$, two-tailed Mann–Whitney *U*) (Fig. 5*B*). Faster uEPSP kinetics are often attributed to developmental decreases in membrane time constant (Spruston et al., 1994) and/or changes in

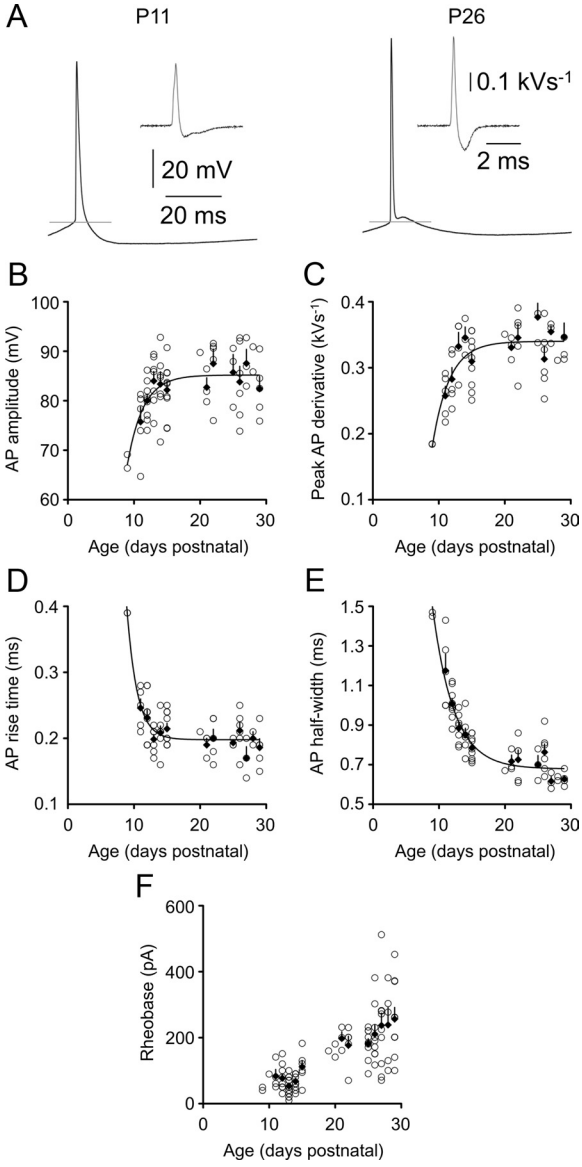

Figure 2. Postnatal development of action potential properties. ***A***, APs recorded in response to a rheobase current stimulus in P11 and P26 animals. Gray lines represent AP threshold, and insets show derivatives of the AP waveform. Calibrations refer to both left and right panels. ***B–F*** show the indicated action potential properties for individual layer 5 pyramidal neurons as a function of animal age. Filled diamonds are averages for each postnatal day. Error bars indicate SEM. In ***B–E***, lines represent single exponential fits to the data.

postsynaptic conductances (Carmignoto and Vicini, 1992; Burgard and Hablitz, 1993; Flint et al., 1997; Stocca and Vicini, 1998; Kumar et al., 2002). In our recordings, the membrane time constant of the postsynaptic cell accounted for a moderate 33% of variance in uEPSP half-width when data were pooled across age groups (Fig. 5*C*). Although we cannot rule out developmental changes in postsynaptic conductances, we observed similar sensitivity to the NMDA receptor antagonist D-APV across the developmental period studied (P25–P29, uEPSP amplitude, 81.7 ± 5.9% of control; half-width, 90.1 ± 9.2%; PPR, 109 ± 11%; $n = 5$; values not significantly different from control; P11–P15, uEPSP amplitude, 78.1 ± 16.1% of baseline; half-width, 79.3 ± 11.9%; PPR, 162 ± 38%; $n = 7$; not significantly different from control). Interestingly, a strong positive correlation between uEPSP half-width and presynaptic AP half-width was ob-

served, with variation in presynaptic AP half-width accounting for 67% of variance in uEPSP half-width (Fig. 5*D*). These data suggest the parallel development of intrinsic and synaptic properties in L5 networks.

Our results above are consistent with a marked developmental change in p_r. As p_r powerfully determines the properties of short-term plasticity at central excitatory synapses (Tsodyks and Markram, 1997; Abbott and Regehr, 2004), we next explored the developmental regulation of excitatory synaptic transmission in response to more complex trains of action potential firing.

Development of paired-pulse plasticity

The postsynaptic response to a standard paired-pulse stimulation protocol (see Material and Methods) showed a dramatic developmental profile (Fig. 6*A*,*B*). In the youngest cortex examined (younger than P11), the second uEPSP of a pair was, on average, larger in amplitude than the first (median paired-pulse ratio, 1.06; mean, 1.40 ± 0.22; range, 0.58–3.0; $n = 13$). The PPR declined to a minimum level at ~P11 (median PPR, 0.71) and was subsequently transformed across postnatal development. At P11–P15, uEPSPs exhibited weak paired-pulse depression (median PPR, 0.95; mean PPR, 1.00 ± 0.049; range, 0.47–2.1; $n = 56$), whereas at P25–P29 the large majority of synapses expressed strong paired-pulse facilitation (48/56 connections; 86%; median PPR, 1.87; mean PPR, 1.91 ± 0.11; range, 0.61–3.87; $n = 56$; significantly different from P11–P15 level; $p < 0.0001$, two-tailed Mann–Whitney *U*) (Fig. 6*C*). Notably, the lowest PPR did not change between the two age groups. Instead, the interconnection variability in PPR increased with development, and the upper end of the PPR distribution shifted toward higher levels of facilitation.

Changes in uEPSP amplitude between the first and second response in a pair (PPR) were similar to changes in indicators of presynaptic release (uEPSP failures and CV) between the first and second response (Fig. 7*A*, traces), supporting a presynaptic locus for paired-paired plasticity across the developmental period studied. The overall proportional change in uEPSP failures between the first and second responses (Fig. 7*B*) was the same as the proportional change in uEPSP amplitude (PPR) (Fig. 6*C*) in both age groups. At P11–P15, uEPSP failures did not change significantly between the first and second uEPSPs (Fig. 7*B*, slope of dotted linear re-

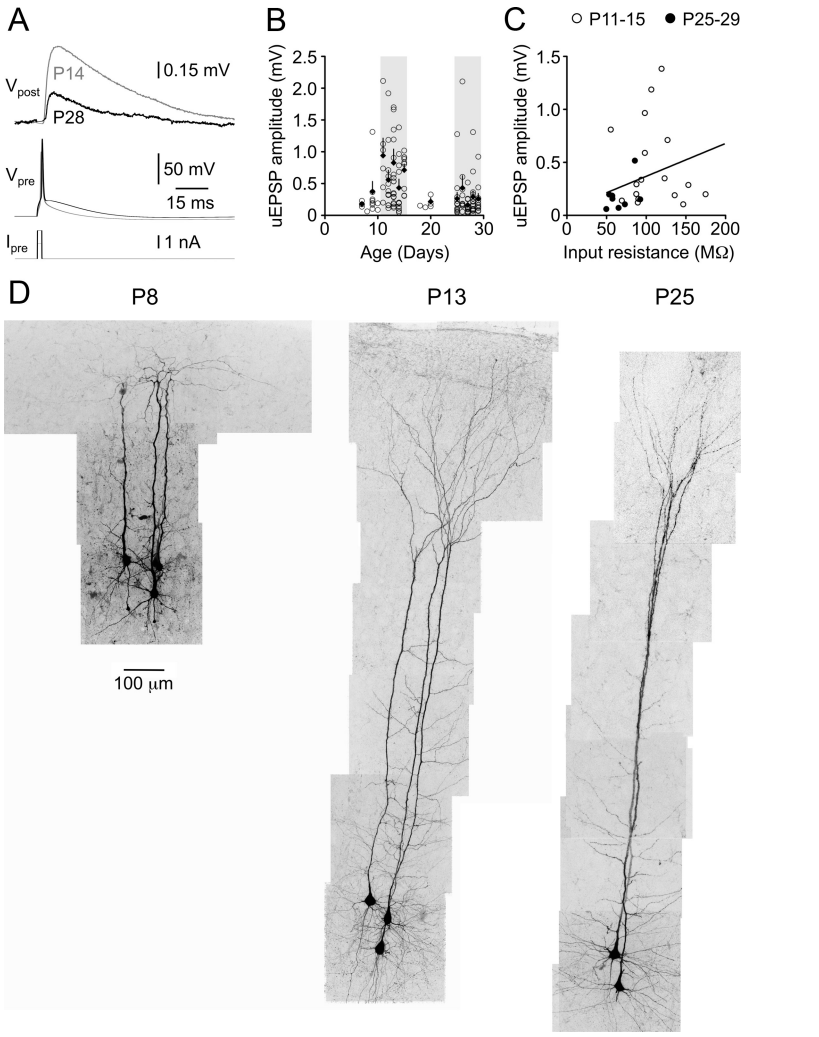

Figure 3. Postnatal development of uEPSP efficacy. ***A***, Averaged layer 5–layer 5 uEPSPs (V_{post}) in response to presynaptic action potentials (V_{pre}) evoked by square-wave current pulses (I_{pre}) in animals aged P14 (gray traces) and P28 (black traces). Calibrations apply to both age groups. ***B***, Mean uEPSP amplitude as a function of animal age (postnatal days). Each data point represents an individual monosynaptic connection. Black diamonds are averages for each postnatal day. Error bars indicate SEM. Light gray shaded regions represent the age ranges selected for detailed analysis, P11–P15 and P25–P29. ***C***, Across the entire data set (open circles, P11–P15; filled circles, P25–P29), uEPSP amplitude was not correlated with postsynaptic apparent input resistance (r^2 of linear regression line, 0.107). ***D***, Confocal reconstructions of small groups of recorded, fluorescently labeled neurons from animals of different ages (P8, P13, and P25) showing rapid changes in neuronal morphology during the developmental period studied.

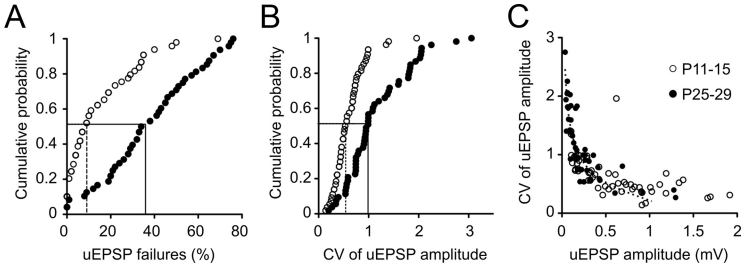

Figure 4. Postnatal development of uEPSP reliability. ***A***, ***B***, Cumulative probability distributions of uEPSP failures (***A***) and the coefficient of variation of uEPSP amplitude (***B***) show an age-related reduction in synaptic reliability (medians indicated by drop lines). ***C***, Relationship between the CV of uEPSP amplitude and uEPSP amplitude for P11–P15 (open circles) and P25–P29 connections (filled circles). Pooled data are well fit by a single binomial equation $CV = \sqrt{[(1 - p_r)/(n_b \cdot p_r)}$, assuming that $CV = \Delta V/(n_b \cdot q_s)$, n_b was fixed at 5.5 release sites, and q_s was set to 0.23 to minimize the sum of squared differences between actual and modeled values (dashed line).

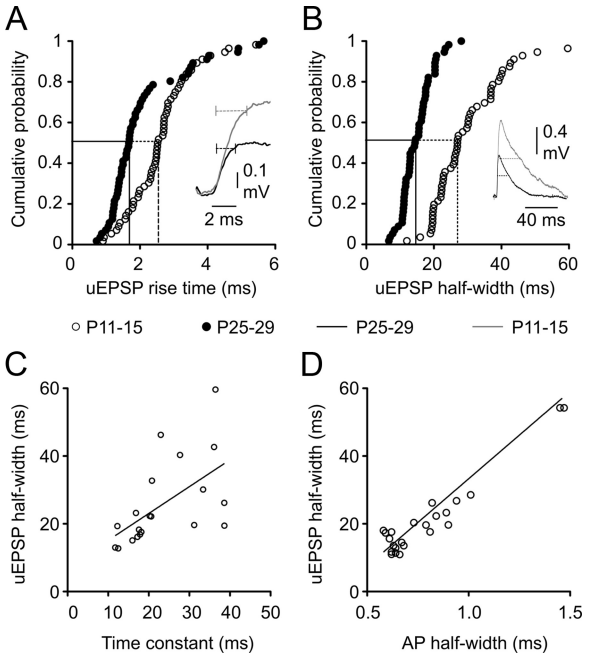

Figure 5. Postnatal development of uEPSP kinetics. ***A***, ***B***, Cumulative probability distributions for mean uEPSP rise time (***A***) and uEPSP half-width (***B***). Dashed drop lines indicate the developmental decreases in the median values. Insets in ***A*** and ***B*** are traces of representative uEPSPs from P11–P15 (gray traces) and P25–P29 (black traces) animals. Dashed horizontal lines in inset in ***A*** indicate a 10–90% rise time of uEPSPs. Dashed horizontal lines in inset in ***B*** indicate the half-width of uEPSPs. ***C***, Relationship between uEPSP half-width and the membrane time constant of the postsynaptic neuron. Each data point represents an individual monosynaptic connection (r^2 of linear regression line, 0.33; $n = 20$). ***D***, Relationship between uEPSP half-width and the half-width of the presynaptic action potential showing a strong positive correlation (r^2 of linear regression line, 0.67; $n = 24$).

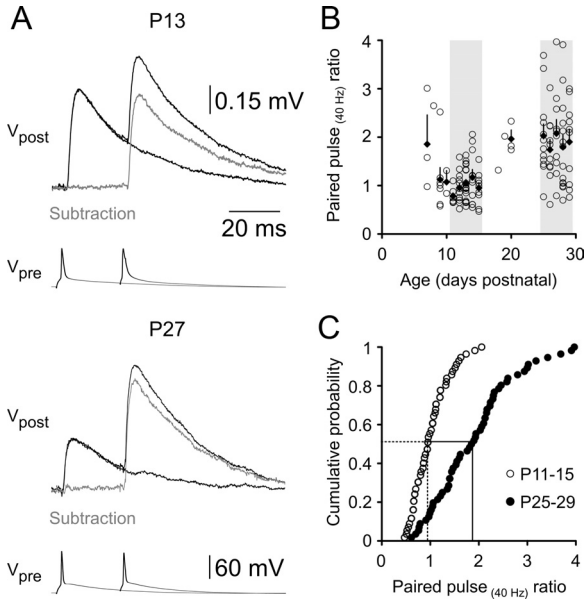

Figure 6. Postnatal development of short-term synaptic plasticity. ***A***, Averaged layer 5–layer 5 uEPSPs (V_{post}) in response to pairs of presynaptic action potentials evoked at a 25 ms interval (V_{pre}) at P13 and P27. Action potential pairs were alternated with single action potentials. Gray traces represent digital subtractions of the single uEPSP waveforms from the doublet uEPSP waveforms. ***B***, PPR as a function of postnatal age. Each data point represents an individual layer 5–layer 5 connection, filled diamonds represent the average PPR for each day with associated SEM values. The light gray shading indicates the two age ranges selected for detailed analysis (P11–P15 and P25–P29). On average, the PPR decreased between P8 and P11 and then increased between P11 and P30. ***C***, Cumulative probability distribution of the PPRs of individual connections showing a doubling in the median PPR (dashed and solid drop lines) between P11 and P15 (open circles) and P25 and P29 (filled circles).

gression line) (not significantly different from 1; $p > 0.05$), consistent with the lack of strong paired-pulse plasticity at this age (Fig. 6*C*, open circles). In animals aged P25–P29, the proportional change in change in uEPSP failures was 1.89 ± 0.28 (Fig. 7*B*, inverse slope of solid black regression line) (failures ratio; $r^2 = 0.659$), the same as the proportional change in uEPSP amplitude (median PPR, 1.87) (Fig. 6*C*, filled circles). A two-way repeated measures ANOVA comparing the CV of the first and second uEPSPs in a pair for each age group revealed a significant interaction between uEPSP number and age. In animals aged P11–P15, where minimal paired-pulse plasticity was observed, the CV did not change significantly between the first and second uEPSPs in a pair (mean first uEPSP CV, 0.605 ± 0.05, $n = 45$; mean second uEPSP CV, 0.622 ± 0.053, $n = 45$; $p > 0.05$, Bonferroni post-test). In contrast, the CV decreased by >40% in P25–P29 animals (mean first uEPSP CV, 1.14 ± 0.094, $n = 42$; mean second uEPSP CV, 0.650 ± 0.037, $n = 42$; $p < 0.0001$, Bonferroni post-test), which expressed strong paired-pulse facilitation.

Presynaptic plasticity can involve a change in either release probability, p_r, or the number of release sites, n. Assuming binomial transmitter release, the locus of expression of synaptic plasticity can be determined by plotting the proportional change in the inverse square of the CV ($CV^{-2}_{uEPSP2}/CV^{-2}_{uEPSP1}$) against the proportional change in the uEPSP amplitude (PPR) (for details of CV analysis of synaptic plasticity, see Faber and Korn, 1991). According to the binomial model, $CV^{-2} = [n \cdot p_r/(1 - p_r)]$, and the mean uEPSP amplitude $m = n \cdot p_r \cdot q$, where n is the number of transmitter release sites, p_r is the probability of transmitter release, and q is the quantal amplitude. When the proportional change in CV^{-2} associated with the induction of synaptic plasticity is greater than the proportional change in m, it therefore suggests a presynaptic change in release probability (as n is common to both terms and CV^{-2} is independent of q). In our experiments, a large majority of facilitatory connections displayed a slope >1 (Fig. 7*C*, points above dashed diagonal line) (13 of 19 facilitating P11–P15 connections; 32 of 36 facilitating P25–P29 connections), suggesting that an increase in p_r underlies facilitation in these pairs of neurons. Approximately half of depressing connections had a slope <1 (Fig. 7*C*, points below dashed diagonal line) (12 of 26 depressing P11–P15 connections; 3 of 6 depressing P25–P29 connections), consistent with a reduction in p_r associated with paired-pulse depression. We cannot, however, rule out a developmental change in the number of transmitter release sites. Indeed anatomical evidence suggests that the number of excitatory synapses in rodent visual cortex does not reach mature levels until P20 (Blue and Parnavelas, 1983). Our data, however, indicate that a developmental regulation of *pr* is the dominant factor shaping the maturational shift toward paired-pulse facilitation at intralaminar L5–L5 synapses. This conclusion is supported by our finding that the relationship between the CV of uEPSPs and amplitude is well described by an equation assuming a constant number of release sites across the developmental period studied (Fig. 4*C*). As L5 neurons are among the first cortical neurons to reach their final laminar position during cortical formation, it seems plausible that the number of intralaminar L5 connections stabilizes earlier in development when compared to other intracortical excitatory connections.

Relationship between eye opening and modification of paired-pulse parameters

On closer inspection, the relationship between use-dependent synaptic plasticity (PPR) and age revealed a biphasic profile (Fig. 6*B*), which was the inverse of the biphasic developmental trend in uEPSP amplitude (Fig. 3*B*). PPR decreased until ~P11, followed by an abrupt change to increasing PPR throughout the rest of the developmental period studied (Fig. 6*B*). The median age at eye opening, documented in a subset of 141 animals, was 11.8 ± 0.09 d postnatal (Fig. 7*D*). We thus postulated that the two phases of PPR development could be temporally related to eye opening. When PPR was considered as a function of age and eye status (open or closed), there was a notable negative correlation between PPR and postnatal age in animals whose eyes were closed at euthanasia, whereas a positive correlation between PPR and postnatal age occurred after eye opening (Fig. 7*E*) (slopes are significantly different; $p = 0.001$). Some caution is needed in interpreting these data, as the number of connections in the "eyes closed" category was small, and the strength of the linear correlation for each age group was low ($r^2 = 0.294$ for animals with closed eyes, 0.268 for animals with open eyes). These data suggest that the onset of visual input may be an important factor shaping the postnatal development of synaptic dynamics in the visual cortex.

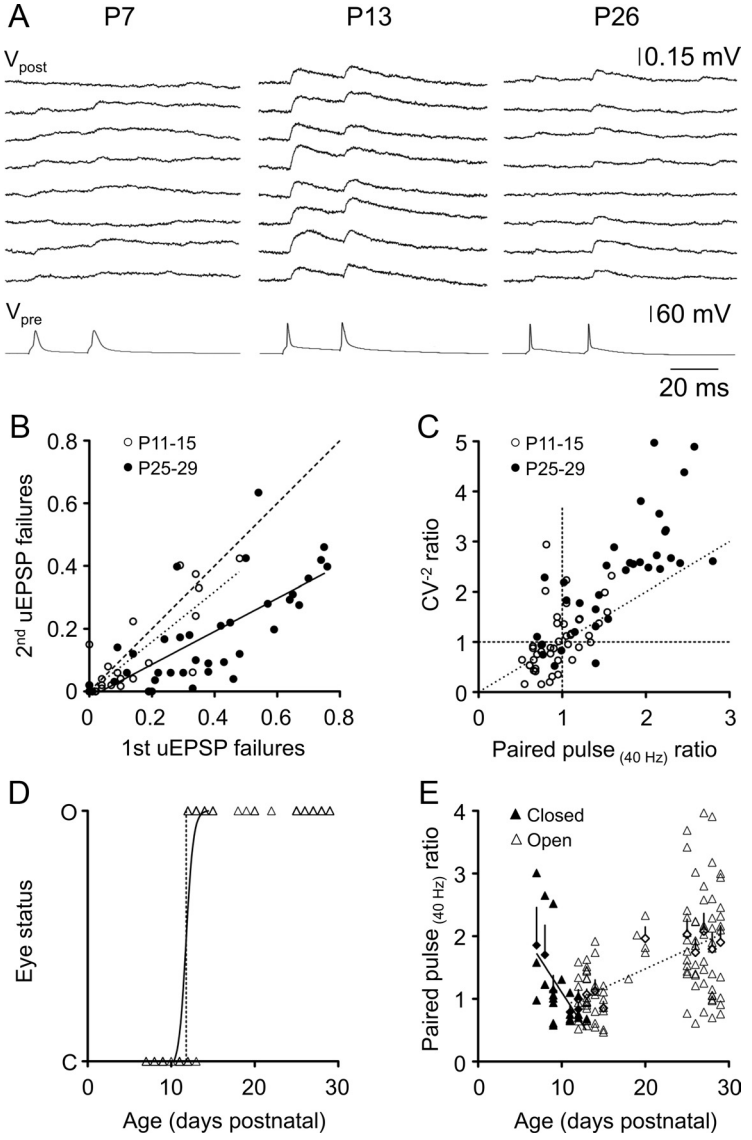

Figure 7. Short-term synaptic plasticity is expressed presynaptically at layer 5 connections across the first postnatal month. ***A***, Representative layer–layer 5 uEPSPs (V_{post}) in response to pairs of presynaptic action potentials (V_{pre}) evoked by square-wave current pulses in animals aged P7 (left), P13 (middle), and P26 (right). Calibration applies to all age groups. ***B***, Relationship between failures of the first and second uEPSPs in a pair for individual layer 5 connections. Filled circles represent P25–P29 connections, and open circles represent P11–P15 connections. The dashed line is an equity line, whereas the solid black line is a linear regression line fit to the P25–P29 data points (slope, 0.567 ± 0.078; $r^2 = 0.558$; $n = 38$), and the dotted black line is a linear regression line fitted to the P11–P15 data points (slope, 0.799 ± 0.11; $r^2 = 0.659$; $n = 26$). ***C***, Relationship between the inverse square of the CV (CV^{-2}) and paired-pulse ratio for P11–P15 (open circles) and P25–P29 (filled circles) connections. Most data points for facilitating connections had slopes above 1 (slope of the dashed line, 1), and approximately half of the data points for depressing connections had slopes <1, suggesting a presynaptic locus for paired-pulse plasticity. ***D***, Summary of eye status (C, closed; O, open) as a function of postnatal age. The black line is a sigmoidal relationship fitted to the data ($r^2 = 0.826$; $n = 141$; age at which 50% of animals' eyes are open, 11.8 ± 0.09 d). ***E***, PPR as a function of postnatal age. Filled triangles represent individual monosynaptic connections from animals whose eyes were closed at the time of euthanasia; open triangles represent animals whose eyes were open before euthanasia. PPR is negatively correlated with postnatal age in animals before eye opening (solid regression line; $r^2 = 0.294$; $n = 22$), but positively correlated with postnatal age after eye opening (dashed regression line; $r^2 = 0.268$; $n = 100$).

Development of frequency tuning

Characterization of synaptic dynamics at intracortical connections has often been restricted to very brief stimulus trains at relatively limited frequencies (Angulo et al., 1999; Reyes and Sakmann, 1999; Zhang, 2004; Ali et al., 2007; Frick et al., 2007a; Oswald and Reyes, 2008), whereas *in vivo* studies have documented neocortical neurons firing for sustained periods at high frequencies (50 Hz or higher) (Hubel and Wiesel, 1959; Porter, 1970; Buracas et al., 1998; deCharms et al., 1998; Shadlen and Newsome, 1998; Steriade et al., 2001; Krupa et al., 2004; Chen and Fetz, 2005; Luna et al., 2005). Understanding the role of L5 connections in the developing cortical circuit therefore requires investigation of synaptic transmission during more complex stimulus trains (Markram and Tsodyks, 1996; Williams and Atkinson, 2007).

We investigated the development of frequency tuning by generating trains of 50 presynaptic APs at fixed frequencies from 0.2 to 50 Hz. At P11–P15, uEPSP amplitude depressed rapidly to a plateau level within less than four stimuli (see representative traces from 10 and 50 Hz stimulus trains) (Fig. 8*A*, *B*, summary). The magnitude of the depression and its rate of onset increased with increasing stimulus frequency (Fig. 8*B*, top). In contrast, P25–P29 L5 connections reliably generated uEPSPs throughout stimulus trains (see representative traces from 10 and 50 Hz stimulus trains) (Fig. 8*A*). Strong facilitation at the start of each train was followed by a decline in uEPSP amplitude; however, the average amplitude stayed about the baseline level throughout the

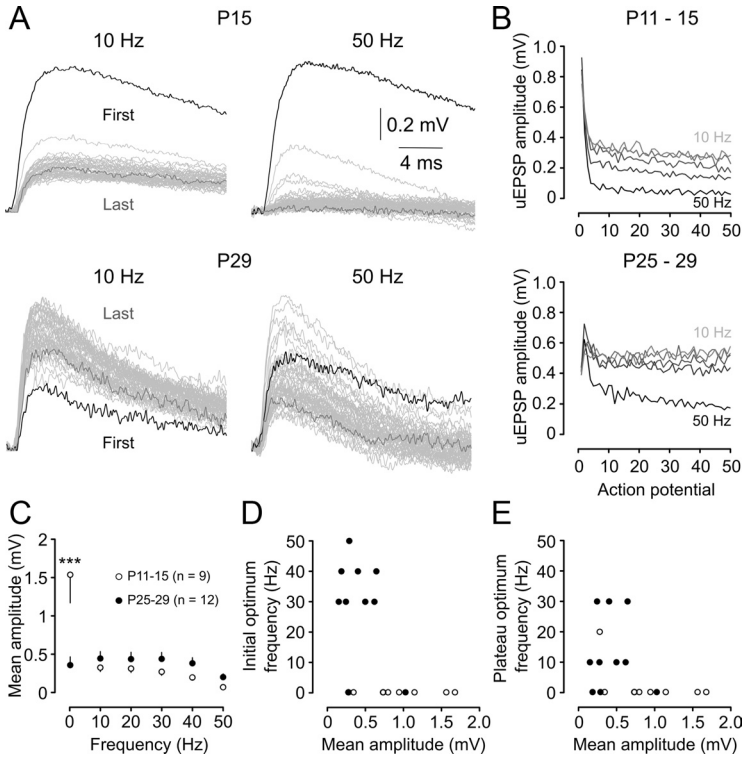

Figure 8. Postnatal development of frequency tuning. ***A***, Averaged uEPSPs recorded from layer 5 pyramidal neurons at two ages (P15 and P29) in response to 50 regularly spaced presynaptic action potentials evoked at the indicated frequencies. Responses to each action potential are overlain, with the first uEPSP in the train shaded black and the last uEPSP in the train shaded dark gray (intervening uEPSPs are shaded light gray). Scale bars apply to both panels. ***B***, Summary of average uEPSP amplitudes for P11–P15 connections ($n = 10$; top), showing the decline in average uEPSP amplitude as a function of action potential number within the train. Increasing stimulus frequency is indicated by increasing intensity of the gray lines (10, 20, 30, 40, and 50 Hz) and is associated with stronger, more rapidly emerging depression. Bottom graph shows mean uEPSP amplitude as a function of action potential number during a 50-pulse train in P25–P29 neurons ($n = 10$). ***C***, Maturation of frequency dependence of action potential train transmission. The mean uEPSP amplitude across the train was largely independent of stimulus frequency at P25–P29 (filled circles). In contrast, P11–P15 connections showed prominent low-pass filtering, with much higher mean uEPSP amplitudes observed at 0.2 Hz. A two-way ANOVA comparing the frequency dependence of uEPSP amplitudes in the two groups revealed a significant interaction between age and stimulation frequency. Asterisks indicate a significant difference between P11–P15 and P25–P29 uEPSP amplitudes at 0.2 Hz (***$p < 0.001$; Bonferroni post-test). ***D***, Optimum frequency, defined as the frequency at which the maximum mean uEPSP amplitude of the first five uEPSPs in the train, was observed for each connection as a function of mean uEPSP amplitude for each connection at its optimum frequency. Filled circles represent connections from P25–P29 animals; open circles represent connections from P11–P15 animals. ***E***, Same as ***D*** except that optimum frequency was determined from the average amplitude of the last five uEPSPs in the train.

train except at the highest frequency studied (50 Hz) (Fig. 8*B*, bottom).

When uEPSP amplitude was averaged across each of the 50 stimuli in a train, P25–P29 synapses displayed approximately the same efficacy across a wide range of stimulus frequencies (from 0.2 to 40 Hz) (Fig. 8*C*, filled circles). Similar bandpass behavior of juvenile L5 connections has been reported in somatosensory cortex (Williams and Atkinson, 2007). There was no significant difference in average uEPSP amplitude between P11–P15 and P25–P29 neurons for frequencies between 10 and 50 Hz, with young L5 connections also transmitting uEPSPs with similar efficacy across this frequency range (Fig. 8*C*, open circles). However, a marked difference between the two age groups was observed at very low frequency (0.2 Hz); the average P11–P15 uEPSP amplitude at 0.2 Hz was more than threefold greater than both the average P25–P29 uEPSP amplitude at this frequency and the P11–P15 uEPSP amplitude at all of the other frequencies tested. Thus, immature L5 connections are only able to maintain their very high synaptic efficacy during low-frequency stimulus trains, whereas strong depression during higher-frequency stimulus trains dramatically reduces the average uEPSP amplitude.

The strong tuning of very young L5 connections to transmit low-frequency signals, regardless of the average uEPSP amplitude, was emphasized by plotting the optimum frequency [defined as the stimulation frequency that led to the highest average uEPSP amplitude in either the first five (Fig. 8*D*, open circles) or last five (Fig. 8*E*, open circles) stimuli in a train] as a function of uEPSP amplitude for each connection. By P25–P29, a much more diverse range of optimum firing frequencies emerged, with a range of connections with different efficacies sharing each of the optimum frequency bands (Fig. 8*D*, filled circles). The variability in optimum frequency between different P25–P29 connections was maintained throughout the AP train (Fig. 8*E*).

Development of synaptic transmission evoked by complex action potential trains

The use-dependent properties of synaptic transmission are particularly important for shaping information transfer at cortical connections in an activity- and frequency-dependent manner (for review, see Feldmeyer and Radnikow, 2009). We thus explored how connections in the two age groups process more complex, time-varying patterns of presynaptic AP firing.

Excitatory transmission at each synaptic connection was investigated in response to three different stimulus protocols, involving trains of 50 presynaptic APs with the same mean frequency (10 Hz) but a wide range of instantaneous frequencies. The "regular" protocol was a fixed-frequency (10 Hz) AP train (Fig. 9*A*, top traces), the "Poisson" protocol involved AP delivered at times derived from a modified Poisson distribution with instantaneous AP frequencies ranging from 2–250 Hz (Fig. 9*A*, middle) (for details of instantaneous frequency distributions, see Williams and Atkinson, 2007), and the "burst" protocol involved bursts of 10 APs with an intraburst frequency of 50 Hz (Fig. 9*A*, bottom).

Despite the marked maturational changes in neuronal and synaptic properties, L5 connections in both age groups transmitted the different stimulus patterns with approximately the same average efficacy (as measured by cumulative within train uEPSP amplitude) (Fig. 9*B*) ($p > 0.05$; two-way ANOVA for effect of age and stimulus pattern), similar to the behavior of juvenile L5 connections in somatosensory cortex (Williams and Atkinson, 2007). There was a nonsignificant trend for P11–P15 connections to transmit Poisson trains more efficaciously than either regular or bursting trains. This is most likely because short AP intervals during the Poisson AP train promote more temporal summation than occurs during a regular train, while less frequency-dependent depression of uEPSP amplitudes would be engaged during Poisson than burst protocols because of the relatively low

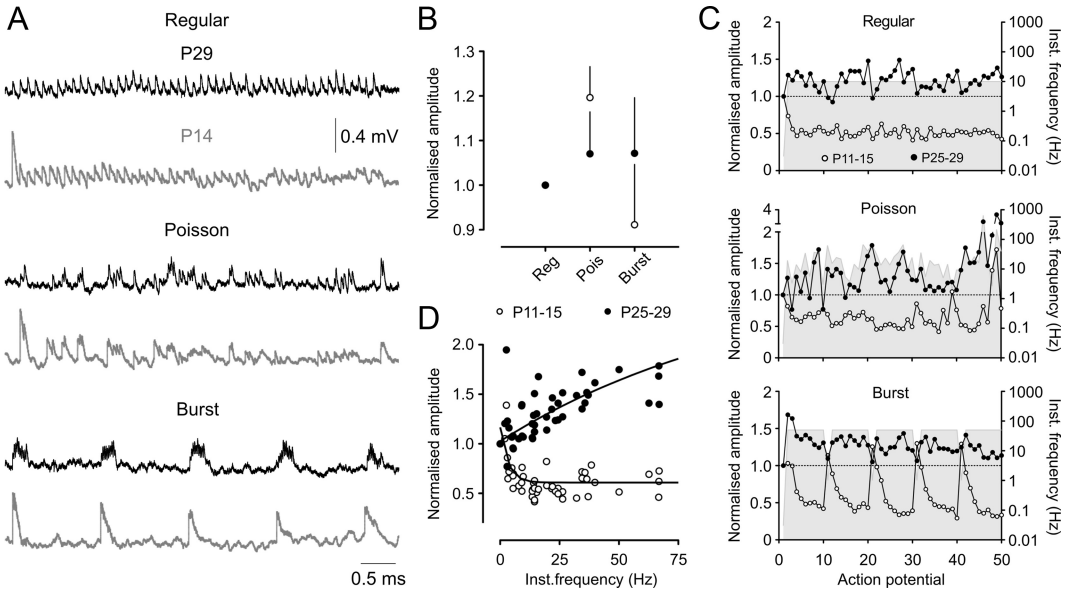

Figure 9. Postnatal development of synaptic transmission evoked by complex action potential trains. ***A***, Averaged uEPSP amplitudes from P29 (black traces) and P14 (gray traces) layer 5 pyramidal connections evoked by 50 presynaptic action potentials with the same mean frequency (10 Hz) but different temporal patterns of AP firing. ***B***, Averaged cumulative uEPSP amplitudes for each stimulus protocol, expressed relative to the regular protocol level. There was no significant difference between P11–P15 (open circles; $n = 9$) and P25–P29 (filled circles; $n = 7$) connections in the normalized values for any of the stimulus protocols. ***C***, Averaged uEPSP amplitudes, normalized to the first uEPSP in the train, expressed as a function of action potential number for the regular, Poisson, and burst stimulus protocols. P11–P15 connections ($n = 9$) and P25–P29 ($n = 7$) connections are represented by open and filled circles, respectively. The gray shading represents the instantaneous stimulus frequency at each point in the train, quantified on the right ordinate axis. ***D***, Relationship between average uEPSP amplitude, normalized to the first uEPSP in the train, and instantaneous action potential frequency during Poisson stimulus trains in P11–P15 ($n = 9$; open circles) and P25–P29 ($n = 7$; filled circles) connections.

median firing frequency (median Poisson AP frequency, 16.1 Hz, vs 49.5 Hz for the burst protocol).

Contrastingly, marked differences between the age groups were apparent when uEPSP amplitudes were considered as a function of stimulus number within a complex train. Train and burst onset was signaled strongly by P11–P15 connections across all three protocols, due to the large initial uEPSP amplitude (Fig. 9*A*, gray traces, *C*, open circles). Transmission during one or two subsequent APs was maintained by significant temporal summation resulting from the long uEPSP time course. However, uEPSP amplitude depressed rapidly with maintained stimulation. By contrast, P25–P29 connections displayed overall facilitation during complex AP trains and reliably transmitted the duration of each stimulus protocol (although some depression of uEPSPs was observed during the bursting protocol) (Fig. 9*A*, black traces, *C*, filled circles). Thus, L5 connections in young cortex (P11–P15) are optimally suited to signaling stimulus onset and short or very low-frequency bursts of AP firing, with the capacity for efficacious transmission of longer AP trains across a wider range of frequencies emerging over the next two postnatal weeks.

Frequency-dependent synaptic modification is an important contributor to information flow in cortical circuits (Galarreta and Hestrin, 1998; Fuhrmann et al., 2002; Beck et al., 2005; Williams and Atkinson, 2007). When uEPSP amplitude, normalized to the first uEPSP, was plotted as a function of instantaneous AP frequency during the Poisson train, steep frequency-dependent depression in uEPSP amplitudes with increasing instantaneous frequency was observed in P11–P15 animals (Fig. 9*D*, open circles). In contrast, a reasonably strong positive relationship between instantaneous presynaptic AP firing frequency and uEPSP amplitude was apparent at P25–P29 (Fig. 9*D*, filled circles). Use-dependent synaptic dynamics are therefore operational throughout prolonged AP trains at L5 connections. The observed maturational changes in use-dependent synaptic dynamics indicate that L5–L5 excitatory synapses function as low-pass filters during sustained activity in P11–P15 animals, but effectively signal the temporal characteristics of prolonged AP firing patterns before the end of the first postnatal month.

Discussion

Here we investigated the postnatal development of the intrinsic properties and intracortical synaptic transmission between large, thick-tufted, pyramidal neurons of rodent visual cortex. The main finding of the present study is that, through a refinement of intrinsic and synaptic properties, the capacity of the L5 excitatory network to transmit the temporal information encoded in action potential firing patterns is transformed over the first postnatal month.

In the visual cortex, functional retinotopic and ocular dominance maps are formed before eye opening and are refined during postnatal development (White and Fitzpatrick, 2007). How might the documented developmental changes in intrinsic and synaptic properties affect the function of the L5 neural network of the visual cortex? We find that the properties of excitatory synaptic transmission between L5 pyramidal neurons at a developmental stage before eye opening can be characterized as weak and unreliable. However, contemporaneously with eye opening, we find a dramatic shift in the properties of excitatory synaptic transmission, to uEPSPs of large amplitude that are reliable from trial to trial when evoked at low repetition frequencies. At this developmental stage (P11–P15), L5 neurons also exhibit a long membrane time constant. In concert with the large amplitude and slow kinetics of uEPSPs, this will act to maximize the temporal summation of synaptic potentials and so promote activity-dependent stabilization of salient connections during cortical map refinement, consistent with findings from the somatosensory system (Feldmeyer and Radnikow, 2009). Interestingly, we observed that this transition in the properties of unitary excitatory synaptic

transmission was accompanied by a marked and rapid development of the properties of presynaptic action potentials, which approached mature values by P15. These data suggest that during early postnatal development, the enhanced reliability of synaptic transmission may be related to more faithful axonal propagation of presynaptic action potentials.

The properties of uEPSPs were further refined through postnatal development, exhibiting a progressive reduction in amplitude, accompanied by an increase in failure rate and a transformation of the properties of short-term, use-dependent plasticity, which reached a plateau in the fourth postnatal week. This refinement of the properties of unitary excitatory synaptic transmission was more marked in the present study than reported for other excitatory intracortical synapses (cf. Frick et al., 2007b). Moreover, the unexpected biphasic age-dependent maturation of synaptic strength and short-term plasticity observed here is absent (Chen and Roper, 2004; Zhang, 2004; Oswald and Reyes, 2008) or less rapid (Frick et al., 2007a,b) in other published accounts of the development of unitary excitatory transmission in the neocortex. It is possible that the day-by-day investigation of synaptic properties in the present study has revealed a biphasic trend that occurs in other cortices but was obscured in previous studies by pooling data across wide age ranges. However, as the shift in development of synaptic properties was contemporaneous with eye opening, an alternative interpretation of these findings is that the rapid change in synaptic properties in visual cortex is related to the alteration in sensory input to visual cortex associated with postnatal eye opening.

After postnatal eye opening, alterations in the properties of unitary excitatory synaptic transmission were paralleled by a refinement of the intrinsic electrophysiological properties of L5 pyramidal neurons, which reached mature levels over the same time period. During this developmental period, we observed a strong downregulation of release probability at L5–L5 pyramidal neuron synapses. This developmental change transformed the ability of L5 neuronal networks to transmit complex patterns of action potential firing. At developmental time points closely following eye opening, pronounced use-dependent short-term depression ensured that only low-frequency trains of action potentials were transmitted without decrement. In contrast, by the fourth postnatal week, high-frequency AP trains evoked uEPSPs without decrement. Indeed, in response to complex, time-varying patterns of action potential firing, with an instantaneous frequency distribution similar to those observed *in vivo* (Holt et al., 1996; Shadlen and Newsome, 1998; Stevens and Zador, 1998), we observed that immature (P11–P15) synapses showed increasing depression as the instantaneous presynaptic action potential firing frequency increased, whereas at P25–P29 we observed increasing facilitation. When taken together with the developmental changes in the intrinsic electrophysiological properties of L5 pyramidal neurons reported here and the parallel development of dendritic electrogenesis and somatodendritic electrical compartmentalization (Atkinson and Williams, 2009), the developmental transformation of unitary excitatory synaptic transmission we observed may contribute to high ongoing action potential firing rates of large L5 pyramidal neurons (De Kock and Sakmann, 2009). This may have particular implications for the emergence of L5 pyramidal neurons as strong drivers of synchronized neocortical network activity (Silva et al., 1991).

Neocortical activity, during certain behavioral states, is dominated by the generation of low-frequency synchronized oscillatory activity (for review, see Castro-Alamancos, 2009). At the single neuron level, this is characterized as a transition between depolarized states (up states), often crowned by action potential firing, and hyperpolarized periods (down states) (Sanchez-Vives and McCormick, 2000; Shu et al., 2003; Crochet and Petersen, 2006; Constantinople and Bruno, 2011). Excitatory synaptic transmission among large L5 pyramidal cells has been shown to be critical for the initiation and propagation of this form of oscillatory activity (Sanchez-Vives and McCormick, 2000; Sakata and Harris, 2009).

Of particular relevance to the present study, synchronized cortical oscillations are the dominant form of coherent activity in the immature rodent cortex and undergo marked developmental regulation. A recent study has investigated changes in up–down state transitions in the mouse visual cortex during the early postnatal period using imaging approaches (Rochefort et al., 2009). Synchronous calcium waves, associated with up states, were not detected before P8, and then showed a rapid developmental increase in frequency and decrease in amplitude, which plateaued within 1 week of eye opening. Contemporaneously, Rochefort et al., (2009) observed a dramatic sparsification in the proportion of cortical neurons engaged in a given up state, from >75% of neurons to only ~10% of neurons active during each wave in mature cortex (Kerr et al., 2005; Rochefort et al., 2009). The emergence of calcium waves in mouse cortex thus occurs 3–4 d before eye opening, and maturation is complete within 1 week, on a similar time scale to the development of L5 intrinsic and synaptic properties described here.

Our results suggest that distinct patterns of activity will engage recurrent, excitatory L5 connections during the second and fourth postnatal weeks, which may contribute to the developmental changes in neocortical oscillatory activity. We observed strong and rapid activity-dependent depression of excitatory synaptic transmission at immature L5–L5 synapses, suggesting that an individual presynaptic neuron would have a restricted ability to dominate the output of its postsynaptic targets during sustained activity. Instead, temporal summation of multiple synaptic inputs is likely to be required to strongly drive recurrent connections in immature L5 networks and may contribute to the infrequent but large-amplitude and widespread distribution of spontaneous cortical oscillations in very young animals. A very different pattern of activation is likely to maximally engage recurrent L5 circuits by the end of the first postnatal month. By this age, the single-stimulus impact of each individual L5 pyramidal neuron on its postsynaptic targets is reduced, due to a fourfold reduction in uEPSP amplitude and significant increase in the current required to initiate action potential firing. However, the emergence of strong, frequency-dependent facilitation in juvenile connections suggests that the somatic impact of an individual synaptic input can increase more than threefold during sustained activity. Thus, our results indicate that recurrent L5 circuits in juvenile cortex will be more effectively recruited by sustained activation in a small population of neurons, which may contribute to the reduced amplitude and spatial sparsification of cortical oscillations observed by Rochefort et al. (2009) in this age range.

In another interesting parallel with our work, Rochefort et al. (2009) showed that the change in visual input with eye opening is a trigger for sparsification of synchronous activity in visual cortex. Furthermore, recent *in vivo* recordings from the cortex of anesthetized rodents and human infants have identified a multiphasic development of evoked and spontaneous cortical activity, where the first immature, evoked responses were observed at P7 in rodents (approximately at the time we first observed functional L5 synaptic connections), followed by a rapid switch to mature evoked responses and higher-frequency spontaneous ac-

tivity 2 d before eye opening at ~P12 (Colonnese et al. 2010). Interestingly, Rochefort et al. (2009) report that dark rearing delayed the onset, but not the progression of age-dependent changes in cortical oscillations, whereas Colonnese et al. (2010) observed no effect of dark-rearing or forced eye opening on the maturation of cortical activity. These studies suggest a potentially complex interaction between eye opening and developmental maturation of synaptic dynamics. It would therefore be informative to ascertain whether there is a causal association between postnatal eye opening and development of synaptic dynamics in visual cortex, and the extent to which any such association is specific to particular intracortical pathways.

Surprisingly few of the extensive investigations of the maturation of synaptic dynamics in sensory cortices have considered the developmental period around the onset of sensory input. The present study has documented major changes in the synaptic dynamics of connections between L5 pyramidal cells across a range of activation patterns in developing rodent cortex and provided data suggesting that a switch in synaptic dynamics may be associated with postnatal eye opening. This work presents a potential mechanism for linking sensory input with maturation of synaptic dynamics in excitatory circuits within neocortical L5, and therefore with developmental changes in the initiation and propagation of spontaneous cortical oscillations.

References

Abbott LF, Regehr WG (2004) Synaptic computation. Nature 431:796–803.

Akerman CJ, Smyth D, Thompson ID (2002) Visual experience before eye-opening and the development of the retinogeniculate pathway. Neuron 36:869–879.

Albert J, Nerbonne J (1995) Calcium-independent depolarization-activated potassium currents in superior colliculus-projecting rat visual cortical neurons. J Neurophysiol 73:2163–2178.

Ali AB, Bannister AP, Thomson AM (2007) Robust correlations between action potential duration and the properties of synaptic connections in Layer 4 interneurones in neocortical slices from juvenile rats and adult rat and cat. J Physiol 580:149–169.

Angulo M, Staiger J, Rossier J, Audinat E (1999) Developmental synaptic changes increase the range of integrative capabilities of an identified excitatory neocortical connection. J Neurosci 19:1566–1576.

Atkinson SE, Williams SR (2009) Postnatal development of dendritic synaptic integration in rat neocortical pyramidal neurons. J Neurophysiol 102:735–751.

Beck O, Chistiakova M, Obermayer K, Volgushev M (2005) Adaptation at synaptic connections to Layer 2/3 pyramidal cells in rat visual cortex. J Neurophysiol 94:363–376.

Blue ME, Parnavelas JG (1983) The formation and maturation of synapses in the visual cortex of the rat. II. Quantitative analysis. J Neurocytol 12:697–712.

Buracas G, Zador A, DeWeese M, Albright T (1998) Efficient discrimination of temporal patterns by motion-sensitive neurons in primate visual cortex. Neuron 20:959–969.

Burgard EC, Hablitz JJ (1993) Developmental changes in NMDA and non-NMDA receptor-mediated synaptic potentials in rat neocortex. J Neurophysiol 69:230–240.

Carmignoto G, Vicini S (1992) Activity-dependent decrease in NMDA receptor responses during development of the visual cortex. Science 258:1007–1011.

Castro-Alamancos M (2009) Cortical up and activated states: implications for sensory information processing. Neuroscientist 15:625–634.

Chen D, Fetz E (2005) Characteristic membrane potential trajectories in primate sensorimotor cortex neurons recorded *in vivo*. J Neurophysiol 94:2713–2725.

Chen HX, Roper SN (2004) Tonic activity of metabotropic glutamate receptors is involved in developmental modification of short-term plasticity in the neocortex. J Neurophysiol 92:838–844.

Chiu C, Weliky M (2002) Relationship of correlated spontaneous activity to functional ocular dominance columns in the developing visual cortex. Neuron 35:1123–1134.

Cohen-Cory S (2002) The developing synapse: construction and modulation of synaptic structures and circuits. Science 298:770–776.

Colonnese M, Kaminska A, Minlebaev M, Milh M, Bloem B, Lescure S, Moriette G, Chiron C, Ben-Ari Y, Khazipov R (2010) A conserved switch in sensory processing prepares developing neocortex for vision. Neuron 67:480–498.

Constantinople CM, Bruno RM (2011) Effects and mechanisms of wakefulness on local cortical networks. Neuron 69:1061–1068.

Crochet S, Petersen CCH (2006) Correlating whisker behavior with membrane potential in barrel cortex of awake mice. Nat Neurosci 9:608–610.

deCharms R, Blake D, Merzenich M (1998) Optimizing sound features for cortical neurons. Science 280:1439–1443.

DeFelipe J (1997) Types of neurons, synaptic connections and chemical characteristics of cells immunoreactive for calbindin-D28K, parvalbumin and calretinin in the neocortex. J Chem Neuroanat 14:1–19.

De Kock C, Sakmann B (2009) Spiking in primary somatosensory cortex during natural whisking in awake head-restrained rats is cell-type specific. Proc Natl Acad Sci U S A 106:16446.

Douglas RJ, Martin KAC (2004) Neuronal circuits of the neocortex. Annu Rev Neurosci 27:419–451.

Faber D, Korn H (1991) Applicability of the coefficient of variation method for analyzing synaptic plasticity. Biophys J 60:1288–1294.

Fagiolini M, Pizzorusso T, Berardi N, Domenici L, Maffei L (1994) Functional postnatal development of the rat primary visual cortex and the role of visual experience: Dark rearing and monocular deprivation. Vision Res 34:709–720.

Feldmeyer D, Radnikow G (2009) Developmental alterations in the functional properties of excitatory neocortical synapses. J Physiol 587:1889–1896.

Fiser J, Chiu C, Weliky M (2004) Small modulation of ongoing cortical dynamics by sensory input during natural vision. Nature 431:573–578.

Flint A, Maisch U, Weishaupt J, Kriegstein A, Monyer H (1997) NR2A subunit expression shortens NMDA receptor synaptic currents in developing neocortex. J Neurosci 17:2469–2476.

Franceschetti S, Sancini G, Panzica F, Radici C, Avanzini G (1998) Postnatal differentiation of firing properties and morphological characteristics in layer V pyramidal neurons of the sensorimotor cortex. Neurosci 83:1013–1024.

Frick A, Feldmeyer D, Sakmann B (2007a) Postnatal development of synaptic transmission in local networks of L5A pyramidal neurons in rat somatosensory cortex. J Physiol 585:103–116.

Frick A, Feldmeyer D, Helmstaedter M, Sakmann B (2007b) Monosynaptic connections between pairs of L5A pyramidal neurons in columns of juvenile rat somatosensory cortex. Cereb Cortex 18:397–406.

Fuhrmann G, Segev I, Markram H, Tsodyks M (2002) Coding of temporal information by activity-dependent synapses. J Neurophysiol 87:140–148.

Galarreta M, Hestrin S (1998) Frequency-dependent synaptic depression and the balance of excitation and inhibition in the neocortex. Nat Neurosci 1:587–594.

Golshani P, Goncalves JT, Khoshkhoo S, Mostany R, Smirnakis S, Porter-Cailliau C (2009) Internally mediated developmental desynchronization of neocortical network activity. J Neurosci 29:10890–10899.

Holt GR, Softky WR, Koch C, Douglas RJ (1996) Comparison of discharge variability in vitro and in vivo in cat visual cortex neurons. J Neurophysiol 75:1806–1814.

Hubel D, Wiesel T (1959) Receptive fields of single neurones in the cat's striate cortex. J Physiol 148:574–591.

Huberman A, Feller M, Chapman B (2008) Mechanisms underlying development of visual maps and receptive fields. Annu Rev Neurosci 31:479–509.

Jones E, Wise S (1977) Size, laminar and columnar distribution of efferent cells in the sensory-motor cortex of monkeys. J Comp Neurol 175:391–437.

Kasper E, Lübke J, Larkman A, Blakemore C (1994a) Pyramidal neurons in layer 5 of the rat visual cortex. III. Differential maturation of axon targeting, dendritic morphology, and electrophysiological properties. J Comp Neurol 339:495–518.

Kasper E, Larkman A, Lübke J, Blakemore C (1994b) Pyramidal neurons in layer 5 of the rat visual cortex. II. Development of electrophysiological properties. J Comp Neurol 339:475–494.

Katz L, Shatz C (1996) Synaptic activity and the construction of cortical circuits. Science 274:1133–1138.

Kerr J, Greenberg D, Helmchen F (2005) Imaging input and output of neocortical networks *in vivo.* Proc Natl Acad Sci U S A 102:14063–14068.

Khazipov R, Sirota A, Leinekugel X, Holmes G, Ben-Ari Y, Buzsáki G (2004) Early motor activity drives spindle bursts in the developing somatosensory cortex. Nature 432:758–761.

Krupa D, Wiest M, Shuler M, Laubach M, Nicolelis M (2004) Layer-specific somatosensory cortical activation during active tactile discrimination. Science 304:1989–1992.

Kumar SS, Bacci A, Kharazia V, Huguenard JR (2002) A developmental switch of AMPA receptor subunits in neocortical pyramidal neurons. J Neurosci 22:3005–3015.

Luna R, Hernández A, Brody C, Romo R (2005) Neural codes for perceptual discrimination in primary somatosensory cortex. Nat Neurosci 8:1210–1219.

Markram H, Tsodyks M (1996) Redistribution of synaptic efficacy between neocortical pyramidal neurons. Nature 382:807–810.

Markram H, Lubke J, Frotscher M, Roth A, Sakmann B (1997) Physiology and anatomy of synaptic connections between thick tufted pyramidal neurones in the developing rat neocortex. J Physiol 500:409–440.

McCormick D, Prince D (1987) Post-natal development of electrophysiological properties of rat cerebral cortical pyramidal neurones. J Physiol 393:743–762.

Micheva K, Beaulieu C (1996) Quantitative aspects of synaptogenesis in the rat barrel field cortex with special reference to GABA circuitry. J Comp Neurol 373:340–354.

Oswald A-MM, Reyes AD (2008) Maturation of intrinsic and synaptic properties of layer 2/3 pyramidal neurons in mouse auditory cortex. J Neurophysiol 99:2998–3008.

Porter R (1970) Early facilitation at corticomotoneuronal synapses. J Physiol 207:733–745.

Reyes A, Sakmann B (1999) Developmental switch in the short-term modification of unitary EPSPs evoked in Layer 2/3 and Layer 5 pyramidal neurons of rat neocortex. J Neurosci 19:3827–3835.

Rice D, Barone S Jr (2000) Critical periods of vulnerability for the developing nervous system: evidence from humans and animal models. Environ Health Perspec 108:511–533.

Rochefort N, Garaschuk O, Milos R, Narushima M, Marandi N, Pichler B, Kovalchuk Y, Konnerth A (2009) Sparsification of neuronal activity in the visual cortex at eye-opening. Proc Natl Acad Sci U S A 106:15049–15054.

Sakata S, Harris K (2009) Laminar structure of spontaneous and sensory-evoked population activity in auditory cortex. Neuron 64:404–418.

Sanchez-Vives MV, McCormick DA (2000) Cellular and network mechanisms of rhythmic recurrent activity in neocortex. Nat Neurosci 3:1027–1034.

Shadlen M, Newsome W (1998) The variable discharge of cortical neurons: implications for connectivity, computation, and information coding. J Neurosci 18:3870–3896.

Shu Y, Hasenstaub A, McCormick D (2003) Turning on and off recurrent balanced cortical activity. Nature 423:288–293.

Silva L, Amitai Y, Connors B (1991) Intrinsic oscillations of neocortex generated by Layer 5 pyramidal neurons. Science 251:432–435.

Solomon J, Nerbonne J (1993a) Hyperpolarization-activated currents in isolated superior colliculus-projecting neurons from rat visual cortex. J Physiol 462:393–420.

Solomon J, Nerbonne J (1993b) Two kinetically distinct components of hyperpolarization-activated current in rat superior colliculus-projecting neurons. J Physiol 469:291–313.

Spruston N, Jaffe D, Johnston D (1994) Dendritic attenuation of synaptic potentials and currents: The role of passive membrane properties. Trends Neurosci 17:161–165.

Steriade M, Timofeev I, Grenier F (2001) Natural waking and sleep states: A view from inside neocortical neurons. J Neurophysiol 85:1969–1985.

Stevens CF, Zador AM (1998) Input synchrony and the irregular firing of cortical neurons. Nat Neurosci 1:210–217.

Stocca G, Vicini S (1998) Increased contribution of NR2A subunit to synaptic NMDA receptors in developing rat cortical neurons. J Physiol 507:13–24.

Tsodyks MV, Markram H (1997) The neural code between neocortical pyramidal neurons depends on neurotransmitter release probability. Proc Natl Acad Sci U S A 94:719–723.

van Zundert B, Yoshii A, Constantine-Paton M (2004) Receptor compartmentalization and trafficking at glutamate synapses: A developmental proposal. Trends Neurosci 27:428–437.

Wang Z, McCormick D (1993) Control of firing mode of corticotectal and corticopontine layer V burst-generating neurons by norepinephrine, acetylcholine, and 1S, 3R-ACPD. J Neurosci 13:2199–2216.

White LE, Fitzpatrick D (2007) Vision and cortical map development. Neuron 56:327–338.

Williams SR, Atkinson SE (2007) Pathway-specific use-dependent dynamics of excitatory synaptic transmission in rat intracortical circuits. J Physiol 585:759–777.

Wong R (1999) Retinal waves and visual system development. Neurosci 22:29–47.

Yuste R, Peinado A, Katz L (1992) Neuronal domains in developing neocortex. Science 257:665–669.

Zhang ZW (2004) Maturation of Layer V pyramidal neurons in the rat prefrontal cortex: Intrinsic properties and synaptic function. J Neurophysiol 91:1171–1182.